Kybernetika

Jiří Fürst; Karel Kozel; Petr Furmánek

High order finite volume schemes for numerical solution of 2D and 3D transonic flows

Kybernetika, Vol. 45 (2009), No. 4, 567--579

Persistent URL: http://dml.cz/dmlcz/140059

KYBERNETIKA — VOLUME *45* (2009), NUMBER 4, PAGES 567 – 579

HIGH ORDER FINITE VOLUME SCHEMES FOR NUMERICAL SOLUTION OF 2D AND 3D TRANSONIC FLOWS

Petr Furmánek, Jiří Fürst and Karel Kozel

The aim of this article is a qualitative analysis of two modern finite volume (FVM) schemes. First one is the so called Modified Causon's scheme, which is based on the classical MacCormack FVM scheme in total variation diminishing (TVD) form, but is simplified in such a way that the demands on computational power are much smaller without loss of accuracy. Second one is implicit WLSQR (Weighted Least Square Reconstruction) scheme combined with various types of numerical fluxes (AUSMPW+ and HLLC). Two different test cases were chosen for the comparison −1) two-dimensional transonic inviscid nonstationary flow over an oscillating NACA 0012 profile and 2) three-dimensional transonic inviscid stationary flow around the Onera M6 wing. Nonstationary effects were simulated with the use of Arbitrary Lagrangian–Eulerian Method (ALE). Experimental results for these regimes of flow are easily available and so the numerical results are compared both in-between and with experimental data. The obtained numerical results in all considered cases (2D and 3D) are in a good agreement with experimental data.

Keywords: ALE method, AUSMPW+, Finite Volume Method, HLLC, nonstationary flow, transonic flow, nonstationary flow, TVD

AMS Subject Classification: 76M12, 76H05, 76N99

1. INTRODUCTION

A huge number of new and powerful numerical methods have been proposed in the field of Computational Fluid Dynamics in the last few years. Sometimes they are however enough complicated, which can make their use in a solution of complex problems (as for example nonstationary flows with the fluid-structure interaction or three-dimensional flows) a bit difficult. Therefore two high order FVM schemes based on different approaches (modern TVD and linear reconstruction) were designed in order to maintain simplicity and high level of accuracy in the same time. The schemes were tested on two different inviscid transonic flow regimes (2D nonstationary and 3D stationary) and the numerical results were then compared both in-between and with experimental data.

2. MATHEMATICAL MODEL

Because the chosen flow regime was both in 2D and 3D considered to be inviscid, the system of governing equations is given by the *Euler Equations*, which can be written in the following vector form (2D case):

$$W_t + F(W)_x + G(W)_y = 0, \tag{1}$$

where

$$\begin{aligned} W &= (\rho, \rho u, \rho v, e)^T, \\ F(W) &= (\rho u, \rho u^2 + p, \rho uv, (e+p)u)^T, \\ G(W) &= (\rho v, \rho uv, \rho v^2 + p, (e+p)v)^T. \end{aligned}$$

System (1) is enclosed by the *Equation of State:*

$$p = (\kappa - 1)\Big[e - \frac{1}{2}\rho(u^2 + v^2)\Big], \quad \kappa = \frac{c_p}{c_v}. \tag{2}$$

Meaning of vectors and their components is following: W – vector of conservative variables; $F(W), G(W)$ – inviscid fluxes; ρ – density; (u, v) – velocity vector; p – pressure; e – total energy per unit volume. Subscripts $_t$, $_x$, $_y$ signify time and spatial partial derivatives.

3. NUMERICAL METHODS

System (1) is solved by the Finite Volume Method – the computational domain Ω is divided into a number of quadrilateral cells such that $\Omega = \bigcup_i D_i$, where D_i stays for one cell. In each cell the following relation should be fulfilled (for 2D case):

$$\begin{aligned} &\iint_{D_i} W_t \,\mathrm{d}x\mathrm{d}y + \iint_{D_i} (F(W)_x + G(W)_y)\,\mathrm{d}x\mathrm{d}y \\ &= \iint_{D_i} W_t \,\mathrm{d}x\mathrm{d}y + \oint_{\partial D_i} F(W)dy - G(W)\,\mathrm{d}x \\ &= \iint_{D_i} W_t \,\mathrm{d}x\mathrm{d}y + \oint_{\partial D_i} (F(W), G(W)) \cdot \vec{\mathbf{n}}\,\mathrm{d}S \quad = \quad 0 \end{aligned} \tag{3}$$

where $(F(W), G(W)) \cdot \vec{\mathbf{n}}$ denotes product of a matrix $(F(W), G(W)) \in \mathbb{R}^{4,2}$ and vector $\vec{\mathbf{n}} \in \mathbb{R}^{1,2}$. From this relation the final discrete form of computational scheme is derived. In order to solve the nonstationary type of flows, the Arbitrary Lagrangian–Eulerian method was chosen. Nonstationary formulation of (3) is obtained by integrating the Euler equations over a time dependent control volumes (let them be the computational cells $D_i(t)$).

$$\iint_{D_i(t)} W_t(t)\,\mathrm{d}x\mathrm{d}y + \oint_{\partial D_i(t)} \big(F(W(t)), G(W(t))\big) \cdot \vec{\mathbf{n}}\,\mathrm{d}S = 0. \tag{4}$$

Denoting $W_i(t)$ the mean value of W over the cell $D_i(t)$, using the mean value theorem and applying the identity

$$\frac{\mathrm{d}}{\mathrm{d}t}\iint_{D_i(t)} W(t)\,\mathrm{d}x\mathrm{d}y = \iint_{D_i(t)} W_t(t)\,\mathrm{d}x\mathrm{d}y + \oint_{\partial D_i(t)} W(t)\dot{\mathbf{x}}\cdot\vec{\mathbf{n}}\,\mathrm{d}S, \tag{5}$$

(for detail see [12]) with $\dot{\mathbf{x}} = (\dot{x}_1, \dot{x}_2)$ being the velocity vector of the point x of the boundary $\partial D_i(t)$ and $|D_i(t)|$ the volume of the cell D_i at time t, the following identity is obtained

$$\begin{aligned}\frac{\mathrm{d}}{\mathrm{d}t}(|D_i(t)|W_i(t)) + \oint_{\partial D_i(t)} \Big[\big(F(W(t)), G(W(t))\big) - W(t)\dot{\mathbf{x}}\Big]\cdot\vec{\mathbf{n}}(t)\,\mathrm{d}S \\ \frac{\mathrm{d}}{\mathrm{d}t}(|D_i(t)|W_i(t)) + \oint_{\partial D_i(t)} \big(F^*(W(t)), G^*(W(t))\big)\cdot\vec{\mathbf{n}}(t)\,\mathrm{d}S \quad = \quad 0,\end{aligned} \tag{6}$$

where

$$F^*(W(t)) = F(W(t)) - W(t)\dot{x}_1, \quad G^*(W(t)) = G(W(t)) - W(t)\dot{x}_2. \tag{7}$$

4. NUMERICAL SCHEMES

4.1. Modified Causon's scheme

Numerical solution of (6) and of 3D extension of (1) was obtained by two different FVM schemes. The first was the so called *Modified Causon's scheme* [6]. It is based on classical explicit MacCormack predictor-corrector scheme in TVD form, which is able to deliver very good results. However, it also entails disadvantageous demands for both computational memory and power. Therefore a simplification saving approximately 30 % of computational time was proposed by Causon [2] by introducing a special type of artificial dissipation (AD). This new scheme was still total variation diminishing, but the influence of AD turned out to be particularly strong. The authors on the other hand proposed another modification based on Causon's scheme (referred to as the Modified Causon's scheme), which is keeping advantages of the Causon's scheme while clearing out its drawbacks in the same time. It has the following form:

PREDICTOR:

$$W_{ij}^{n+\frac{1}{2}} = W_{ij}^{n} - \frac{\triangle t}{|D_{ij}|}\sum_{l=1}^{4}(\widetilde{F}_l, \widetilde{G}_l)^n\cdot\vec{S}_l, \tag{8}$$

$$\widetilde{F}_1^n = F(W_{ij}^n), \quad \widetilde{F}_2^n = F(W_{ij}^n), \quad \widetilde{F}_3^n = F(W_{i-1j}^n), \quad \widetilde{F}_4^n = F(W_{ij-1}^n), \tag{9a}$$

$$\vec{S}_1 = \vec{S}_{i+\frac{1}{2}j}, \quad \vec{S}_2 = \vec{S}_{ij+\frac{1}{2}}, \quad \vec{S}_3 = \vec{S}_{i-\frac{1}{2}j}, \quad \vec{S}_4 = \vec{S}_{ij-\frac{1}{2}}. \tag{9b}$$

and vectors $\widetilde{G}$ are given in the same way as vectors $\widetilde{F}$.

CORRECTOR:

$$W_{ij}^{n+1} = \frac{1}{2}\Big[W_{ij}^n + W_{ij}^{n+\frac{1}{2}} - \frac{\triangle t}{|D_{ij}|}\sum_{l=1}^{4}(\widetilde{F}_l, \widetilde{G}_l)^{n+\frac{1}{2}}\cdot\vec{S}_l\Big] + AD(W_{ij}^n). \tag{10}$$

$$\begin{aligned} \widetilde{F}_1^{n+\frac{1}{2}} &= F(W_{i+1j}^{n+\frac{1}{2}}), \qquad & \widetilde{F}_2^{n+\frac{1}{2}} &= F(W_{ij+1}^{n+\frac{1}{2}}), \\ \widetilde{F}_3^{n+\frac{1}{2}} &= F(W_{ij}^{n+\frac{1}{2}}), \qquad & \widetilde{F}_4^{n+\frac{1}{2}} &= F(W_{ij}^{n+\frac{1}{2}}). \end{aligned} \tag{11}$$

Vectors $\widetilde{G}$ and $\vec{S}_{i\pm\frac{1}{2}j\pm\frac{1}{2}}$ are again given in the same way as vectors $\widetilde{F}$. Vectors $\vec{S}_{i\pm\frac{1}{2}j\pm\frac{1}{2}}$ are normal vectors to the interface between the cells i, j and $i \pm 1, j \pm 1$. Their length is equal to the length of this interface and they point "out" of the cell with indices i, j (for detail see Figure 1). $\triangle t$ is the *time step*, which is in the case of explicit Modified Causon's scheme limited by the *CFL* condition [5].

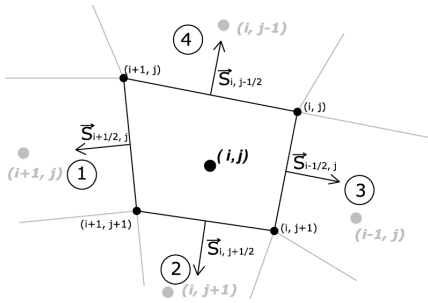

Fig. 1. Global position of cell D_{ij} in structured computational mesh. In this case $\Omega = \bigcup_{ij} D_{ij}$.

In the case of nonstationary flow the scheme itself changes in fact only slightly. In (9a), (9b) and (11) vectors F and G are replaced with vectors F^* and G^* (7).

The Modified Causon's artificial dissipation in (10) is given by

$$AD(W_{ij}^n) = DW_{ij}^1 + DW_{ij}^2,$$

where DW_{ij}^1 is part of artificial dissipation in the direction of index i:

$$\begin{aligned} DW_{ij}^1 \quad = \quad & \left[G^{1+}(r_{ij}^{1+}) + G^{1-}(r_{i+1j}^{1-})\right](W_{i+1j}^n - W_{ij}^n) \\ & - \left[G^{1+}(r_{i-1j}^{1+}) + G^{1-}(r_{ij}^{1-})\right](W_{ij}^n - W_{i-1j}^n), \end{aligned} \tag{12}$$

if we denote $\langle \cdot, \cdot \rangle$ the standard inner (scalar) product in $\mathbb{R}^m$, $m \in \mathbb{N}$, then

$$r_{ij}^{1+} = \frac{\langle W_{ij}^n - W_{i-1j}^n, W_{i+1j}^n - W_{ij}^n \rangle}{\langle W_{i+1j}^n - W_{ij}^n, W_{i+1j}^n - W_{ij}^n \rangle}, \quad r_{ij}^{1-} = \frac{\langle W_{ij}^n - W_{i-1j}^n, W_{i+1j}^n - W_{ij}^n \rangle}{\langle W_{ij}^n - W_{i-1j}^n, W_{ij}^n - W_{i-1j}^n \rangle}, \tag{13}$$

DW_{ij}^2 is given in the same way (in the direction of index j). The remaining functions

are defined as follows:

$$
\begin{aligned}
G^{1,2\pm}(r_{ij}^{1,2\pm}) &= \frac{1}{2}C(\overline{\nu}_{ij}^{1,2})\left[1-\Phi(r_{ij}^{1,2\pm})\right], \quad \Phi(r_{ij}^{1,2\pm}) = \max(0,\min(2r_{ij}^{1,2\pm},1)) \\
C(\overline{\nu}_{ij}^{1,2}) &= \begin{cases} \overline{\nu}_{ij}^{1,2}(1-\overline{\nu}_{ij}^{1,2}) & \text{pro } \overline{\nu}_{ij}^{1,2} \le 0.5 \\ 0.25 & \text{pro } \overline{\nu}_{ij}^{1,2} > 0.5 \end{cases} \\
\overline{\nu}_{ij}^{1} &= \frac{\triangle t}{\triangle x}\Psi(\min(|u'_{ij}-c_{ij}|,|u'_{ij}|,|u'_{ij}+c_{ij}|)), \quad c_{ij} = \sqrt{\kappa\frac{p_{ij}}{\rho_{ij}}} \\
\Psi(x) &= \begin{cases} |x| & \text{pro } |x| > \varepsilon_\epsilon \\ \frac{x^2+\varepsilon_\epsilon^2}{2\varepsilon_\epsilon} & \text{pro } |x| \le \varepsilon_\epsilon, \quad \varepsilon_\epsilon = 10^{-3} \end{cases} .
\end{aligned}
$$

Approximations of the length of i,jth cell in direction i and j are given as

$$\triangle x = \frac{2|D_{ij}|}{|\vec{S}_{i+\frac{1}{2}j} - \vec{S}_{i-\frac{1}{2}j}|}, \tag{14}$$

$$\triangle y = \frac{2|D_{ij}|}{|\vec{S}_{ij+\frac{1}{2}} - \vec{S}_{ij-\frac{1}{2}}|}, \tag{15}$$

and similarly the velocities in directions i and j

$$u'_{ij} = \frac{\left\langle \vec{S}_{i+\frac{1}{2}j} - \vec{S}_{i-\frac{1}{2}j}, (u_{ij}, v_{ij}) \right\rangle}{|\vec{S}_{i+\frac{1}{2}j} - \vec{S}_{i-\frac{1}{2}j}|} \tag{16}$$

$$v'_{ij} = \frac{\left\langle \vec{S}_{ij+\frac{1}{2}} - \vec{S}_{ij-\frac{1}{2}}, (u_{ij}, v_{ij}) \right\rangle}{|\vec{S}_{ij+\frac{1}{2}} - \vec{S}_{ij-\frac{1}{2}}|} \tag{17}$$

with (u_{ij}, v_{ij}) being the velocity vector in cell D_{ij}

4.2. Weighted Least Square Reconstruction scheme (WLSQR)

When solving (6) with the WLSQR scheme, the real inviscid fluxes in the surface integrals are approximated by numerical ones (by the AUSMPW+ flux in the 2D case [11] and by the HLLC flux [1] in 3D case). The resulting FVM scheme is obtained in following way: the equation (3) is rewritten as

$$|D_i|\frac{\mathrm{d}W_i}{\mathrm{d}t} = -\oint_{\partial D_i} (F(W), G(W)) \cdot \vec{\mathbf{n}}\,\mathrm{d}S \tag{18}$$

Again, in the case of nonstationary flow, the vectors F and G are replaced with vectors F^*, G^* (7). The higher order method is obtained by introducing cell-wise interpolation $P(\vec{x};W) = P_i(\vec{x};W),\ \vec{x} \in D_i$ into the basic formula.

$$|D_i|\frac{\mathrm{d}W_i}{\mathrm{d}t} \approx -\sum_{j\in N_i} \mathcal{F}(P_i(\vec{x}_{ij};W), P_j(\vec{x}_{ij};W), \vec{S}_{ij}) \tag{19}$$

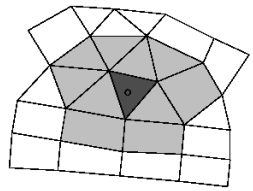

Fig. 2. WLSQR computational stencil.

where $\vec{x}_{ij}$ is the center of interface between cells D_i and D_j, N_i is the set of indices of cells sharing a face with cell D_i. The indices i, j now signify position of the cell D_i and D_j in an unstructured computational mesh. $\mathcal{F}$ denotes the so called numerical flux approximating physical flux through the interface between cells D_i and D_j which is evaluated using interpolated values obtained by cell-wise interpolation polynomial $P(\vec{x}; W)$ (depending on indexes i, j). If we denote the right hand side $-|D_i|R(W)$ the scheme will become

$$\frac{\mathrm{d}W_i}{\mathrm{d}t} = R(W) \tag{20}$$

where $R(W)$ is vector of residuals computed by weighted least square reconstruction and chosen numerical fluxes. Advancing time is solved by the coupled linearized backwards Euler method, which gives

$$\left(I + \Delta t \frac{\partial R^{\mathrm{low}}}{\partial W}\right)\left(W_i^{n+1} - W_i^n\right) = -\Delta t R(W^n)_i. \tag{21}$$

where the high order residual R is replaced by the basic low order residual R^{low} involving only the closest neighborhoods without any reconstruction. The sparse system of linear equations is solved by GMRES with ILU(0) preconditioning. Dimension of the Krylov subspace is chosen between 10 – 40 and maximum number of iteration is set to 10 – 50. If the stationary solution is not found in prescribed number of iterations the computation proceeds in the next time step. The interpolation polynomial itself is obtained by weighted least square method in the following way

$$P_i(\vec{x}; W) := \arg\min \sum_{j \in \mathcal{M}_i} \left(|D_j| W_j - \iint_{D_j} P_i(\vec{x}; W)\, \mathrm{d}x\mathrm{d}y \right)^2 \cdot \mathrm{weight}_{i,j}(W),$$

$$\iint_{D_i} P_i(\vec{x}; W)\, \mathrm{d}x\mathrm{d}y = |D_i| W_i, \quad \mathrm{weight}_{i,j}(W) = \frac{h_{ij}^{-r}}{\left(\frac{|W_i - W_j|}{h_{ij}}\right)^p + h_{ij}^q}$$

$\mathcal{M}_i$ is the set of indices of cells from chosen computational stencil and h_{ij} is distance of centers of gravities of cells D_i and D_j. The weights are data dependent with $p > 0$. Choice of constants p, q, and r might present a problem, but after a number of numerical experiments the optimal range was found. In our case they were chosen as $p = 4, q = -2, r = -3$.

5. NUMERICAL RESULTS

5.1. 2D Nonstationary Transonic Flow

Considered test case is transonic flow over an oscillating NACA 0012 profile for which the experimental data are available in [3]. It is characterized by the inlet Mach number $M_\infty = 0.755$. The oscillatory motion of the profile around the reference point $x_{\text{ref}} = [0.25, 0.00]$ is given by the pitching angle $\alpha_1(t) = 0.016^\circ + 2.51^\circ \sin(\omega t)$. The angular velocity is defined as $\omega = \frac{2kU_\infty}{c}$, where U_∞ is the free-stream velocity (since the non-dimensional form of (1) is considered and angle of attack $\alpha = 0^\circ$ then $U_\infty = M_\infty$), $c = 1$ is the chord length and the reduced frequency $k = 0.0814$. The unsteady state development was observed on the behaviour of the lift coefficient (c_l) given as

$$c_l = \frac{\oint_{\Gamma_{\text{prof}}} p \, \mathrm{d}x}{\frac{1}{2} U_\infty^2 \rho_\infty},$$

where $\rho_\infty = 1$ and Γ_{prof} is the curve defining the profile. The used computational schemes and meshes were

- Modified Causon's scheme – structured C-mesh with 15096 elements (124 cells around profile),
- WLSQR scheme with AUSMPW+ flux – unstructured mesh with 6720 quadrilateral cells (120 cells around profile).

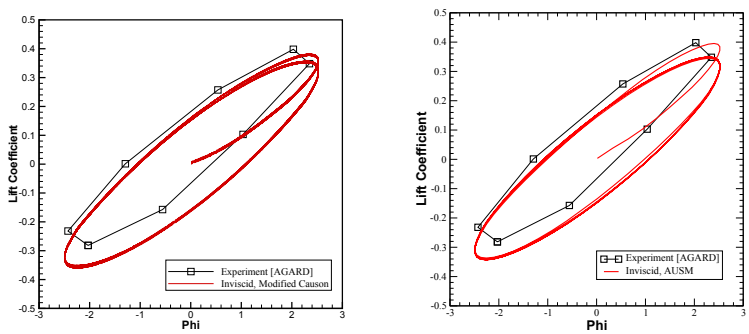

(a) Modified Causon's scheme.

(b) WLSQR scheme with AUSMPW+ flux.

Fig. 3. NACA 0012, lift coefficient behaviour.

Numerical results achieved by both schemes are shown in Figures 3 and 4 in the form of behaviour of the c_l coefficient and distribution of the c_p coefficient.

$$c_p = \frac{p - p_\infty}{\frac{1}{2} U_\infty^2 \rho_\infty}, \quad p_\infty = \frac{1}{\kappa}.$$

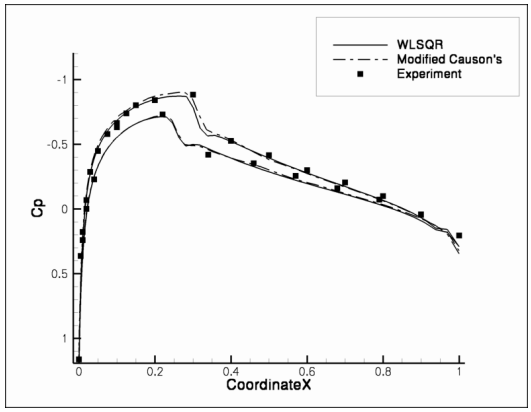

(c) $\alpha_1 = 1.09°$.

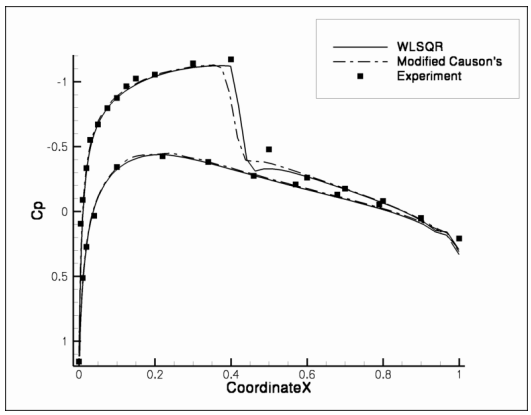

(d) $\alpha_1 = 2.34°$.

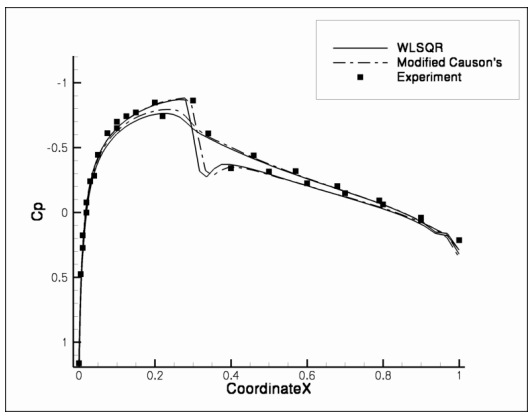

(e) $\alpha_1 = -1.25°$.

Fig. 4. Nonstationary flow over the NACA 0012 airfoil, $M_\infty = 0.755$, $\omega = 0.0814$, comparison of the experimental (AGARD) and numerical results (Modified Causon's and WLSQR scheme).

As can be seen from Figures 3 and 4 the numerical results obtained by both Modified Causon's scheme and WLSQR scheme are very good. In the case of c_l comparison, the results correspond qualitatively, but experimental data show a bit higher c_l values (Figure 3). Considering symmetry of the problem, also the behaviour of the c_l should be symmetric with the center of symmetry in the point $[0, 0]$. The experimental data however do not posses this characteristic and therefore the suspicion of their systematic error comes in mind. Important characteristics, as for example the position and intensity of the shock wave (minimal and maximal reached value of c_p), are however in a very good correspondence.

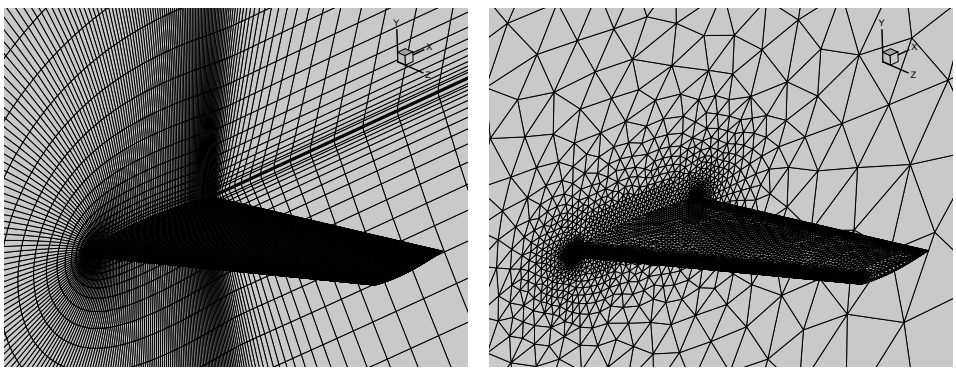

(f) C-mesh. (g) Unstructured mesh.

Fig. 5. Computational meshes.

5.2. 3D Stationary Transonic Flow

In order to compute 3D flow, both schemes were naturally extended to three dimensions. Considered flow regime is well-known test case of transonic flow over the Onera M6 wing characterized by inlet Mach number $M_\infty = 0.8395$ and angle of attack $\alpha = 3.06°$. The experimental data are available in [13]. The used computational schemes and meshes were now

- structured C-mesh with 467313 hexahedral elements (Modified Causon's scheme),
- unstructured mesh with 306843 pyramidal elements (WLSQR scheme with HLLC flux).

Numerical results achieved by both methods in 3D are shown in Figures 6, 7, 8.

Comparison between numerical and experimental results in the case od 3D flow (Figure 8) shows that both schemes give very similar results. The correspondence with experimental data is more than satisfactory (both the position and intensity of shock waves are captured with reasonable accuracy). The observed differences are

highly probable consequence of inviscid nature of the chosen model, which collide with viscous turbulent behaviour of the real flow. The Modified Causon's scheme has somewhat limited use because of its explicit form and its ability to handle only the structured meshes. The first drawback can be removed with using the implicit version of the scheme [14]. Its demands on the computational time are however comparable with the WLSQR scheme, but it needs much less memory (see Table 1).

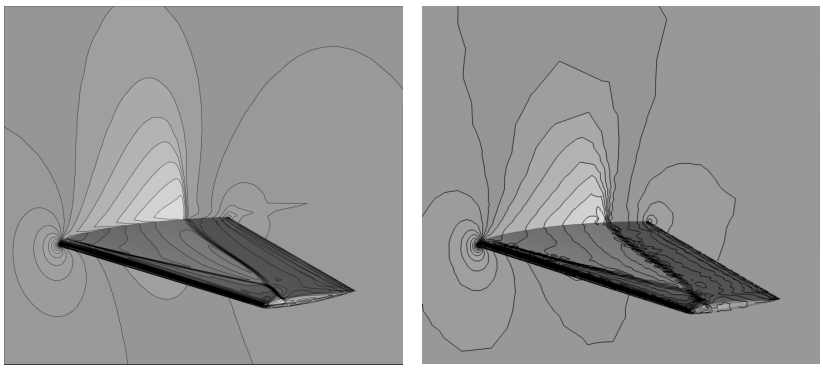

(h) Modified Causon's scheme. (i) WLSQR scheme with HLLC flux.

Fig. 6. Mach number isolines, top side of the wing.

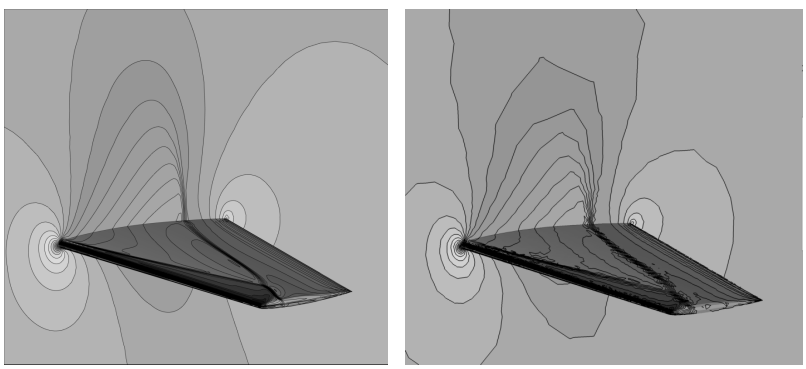

(j) Modified Causon's scheme. (k) WLSQR scheme with HLLC flux.

Fig. 7. c_p coefficient, top side of the wing.

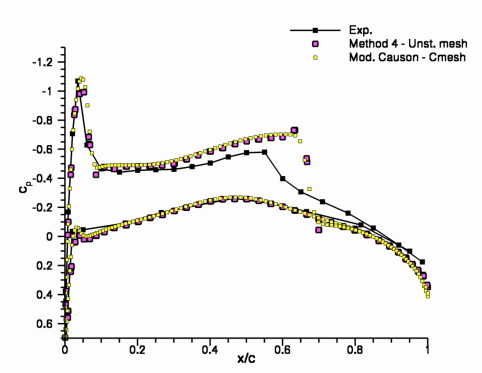

a) 20 % of the wing span

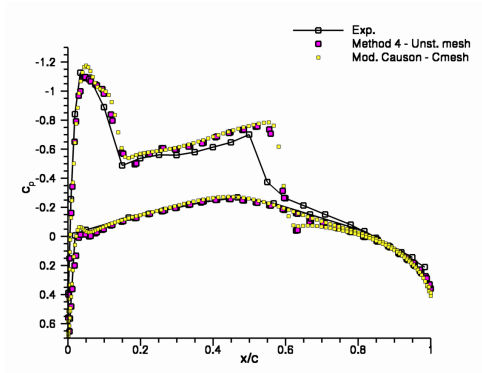

b) 44 % of the wing span

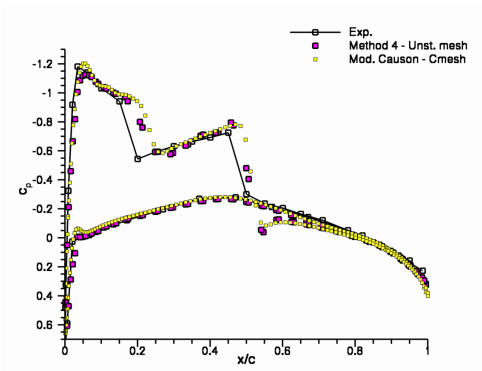

c) 65 % of the wing span

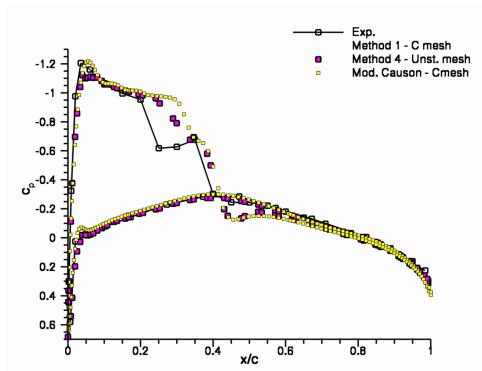

d) 80 % of the wing span

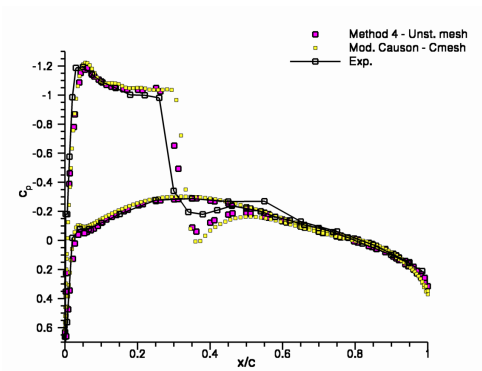

e) 90 % of the wing span

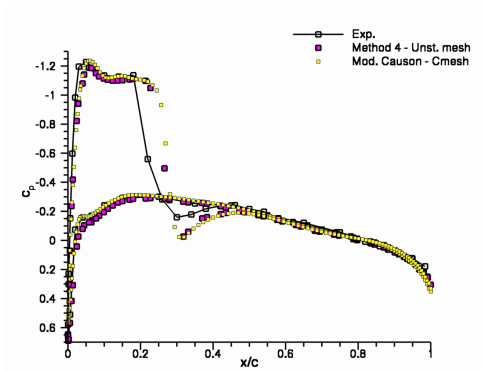

f) 95 % of the wing span

Fig. 8. c_p coefficient behaviour in the cuts along side the wing, comparison of the experimental and numerical results (Modified Causon's scheme and WLSQR scheme – denoted as "Method 4").

WLSQR scheme on the other hand is able to solve greater variety of problems described also by unstructured meshes. Both schemes were implemented in parallel version using the OpenMP library, which acquitted well for their explicit parts (see Table 2). However, this is not the case of the implicit part of the WLSQR scheme (the linear equation solver), which needs to be replaced either by a matrix-free GMRES method or by a cache-optimized version of the solver.

Table 1. Comparison of memory demands of the used schemes (3D flow over the Onera M6 wing).

Scheme	**Memory demand**	**No. of comp. cells**	**Mem. demand with regard to 1 cell**
Modified Causon's Scheme	240 MB	467313	0.513 KB
WLSQR Scheme	850 MB	306843	2.77 KB

Table 2. Parallel efficiency of the used schemes, OpenMP library (3D flow over the Onera M6 wing). AltixXE 320, 2× Intel X5472 (3 GHz).

Scheme	**Number of processors**	**Time for 1 iteration [s]**	**Speedup**	**Efficiency**
Modified Causon's Scheme	1	0.51	1.0	100 %
	8	0.1	5.1	63.75 %
WLSQR Scheme	1	15.9	1.0	100 %
	8	2.8	5.6	70 %

6. CONCLUSION

The proposed FVM schemes for numerical solution of both nonstationary 2D and stationary 3D transonic inviscid flows show very good accuracy and efficiency. Although the inviscid mathematical model have been chosen, the schemes were able to capture important flow characteristics as is the position and intensity of the shock waves and proven themselves as a reliable numerical simulation of investigated cases. Both schemes however would need some further improvement (implicit form in the case of Modified Causon scheme, matrix-free GMRES in the case of WLSQR scheme).

ACKNOWLEDGEMENT

This work was partially supported by the Research Plan VZ MSM 6840770010, VZ MSM 0001066902 and the Czech Science Foundation under Grant 201/08/0012.

(Received October 18, 2008.)

REFERENCES

[1] P. Batten, M. A. Leschziner, and U. C. Goldberg: Average-state Jacobians and implicit methods for compressible viscous and turbulent flows. J. Comput. Phys. *137* (1997), 38–78.

[2] D. M. Causon: High resolution fnite volume schemes and computational aerodynamics. In: Nonlinear Hyperbolic Equations – Theory, Computation Methods and Applications (Notes on Numerical Fluid Mechanics volume 24, J. Ballmann and R. Jeltsch, eds.), Vieweg, Braunschweig 1989, pp. 63–74.

[3] Compendium of Unsteady Aerodynamic Measurements. AGARD Advisory Report No. 702, 1982.

[4] J. Donea: An arbitrary Lagrangian–Eulerian finite element method for transient fluid-structur interactions. Comput. Methods Appl. Mech. Engrg. *33* (1982), 689–723.

[5] M. Feistauer, J. Felcman, and I. Straškraba: Mathematical and Computational Methods for Compressible Flow. (Numerical Mathematics and Scientific Computation.) Oxford University Press, Oxford 2003.

[6] J. Fürst: Numerical Solution of Transonic Flow Using Modern Schemes of Finite volume Method and Finite Differences. Ph.D. Thesis (in Czech), ČVUT, Praha 2001.

[7] J. Fürst: A weighted least square scheme for compressible flows. Submitted to Flow, Turbulence and Combustion 2005.

[8] J. Fürst, M. Janda, and K. Kozel: Finite volume solution of 2D and 3D Euler and Navier–Stokes equations. Math. Fluid Mechanics (J. Neustupa and P. Penel, eds.), Birkhäuser Verlag, Basel 2001.

[9] J. Fürst and K. Kozel: Application of second order TVD and ENO schemes in internal aerodynamics. J. Sci. Comput. *17* (2002), 1–4, 263–272.

[10] J. Fürst and K. Kozel: Second and third order weighted ENO scheme on unstructured meshes. In: Proc. Finite Volumes for Complex Applications III (D. Herbin and D. Kröner, eds.), Hermes Penton Science, pp. 737–744.

[11] Kyu Hong Kim, Chongam Kim, and Oh-Hyun Rho: Methods for the accurate computations of hypersonic flows. AUSMPW+ scheme. J. Comput. Physics *174* (2001), 38–80.

[12] M. Lesoinne and C. Farhat: Geometric conservation laws for flow problems with moving boundaries and deformable meshes, and their impact on aeroelastic computations. Comput. Methods Appl. Mech. Engrg. *134* (1996), 71–90.

[13] V. Schmitt and F. Charpin: Pressure Distributions on the ONERA-M6-Wing at Transonic Mach Numbers. Experimental Data Base for Computer Program Assessment. Report of the Fluid Dynamics Panel Working Group 04, AGARD AR 138, 1979.

[14] H. C. Yee: A Class of High-Resolution Explicit and Implicit Shock-Capturing Methods. Technical Memorandum 101088, NASA, Moffett Field, California 1989.

Petr Furmánek, Jiří Fürst and Karel Kozel, Department of Technical Mathematics, Faculty of Mechanical Engineering, Czech Technical University in Prague, Karlovo nám. 13, 121 35 Praha 2. Czech Republic.
e-mails: Petr.Furmanek@fs.cvut.cz, Jiri.Furst@fs.cvut.cz, kozelk@fsik.cvut.cz